Contents lists available at ScienceDirect

Applied Catalysis B: Environmental

Palladium nanoparticles supported on organosilane-functionalized carbon nanotube for solvent-free aerobic oxidation of benzyl alcohol

Yibo Yan, Yuanting Chen, Xinli Jia, Yanhui Yang*

School of Chemical and Biomedical Engineering, Nanyang Technological University, Singapore 637459, Singapore

ABSTRACT

Palladium nanoparticles supported on carbon nanotubes (CNT) functionalized with various organosilane modifiers have been prepared through a post-synthesis grafting method followed by a metal adsorption–reduction approach. The surface property, catalyst structure, electrochemical activity, and catalytic performance were tested in the selective aerobic oxidation of benzyl alcohol. The variation in type and amount of surface-functional groups played a key role in controlling catalytic behavior through fine tuning the surface basicity, metal nanoparticle size and size distribution, metal–support electronic interaction. In all these tested organosilane modifiers, 3-aminopropyl triethoxysilane exhibited the largest improvement in catalytic performance, with a remarkably high quasi-turnover frequency of 288,755 h^{-1} based on the electrochemical active surface area.

© 2014 Elsevier B.V. All rights reserved.

1. Introduction

Selection oxidation of alcohols to corresponding aldehydes or ketones plays a paramount role in both laboratory and industry on account of the carbonyl versatility in organic synthesis. Extensive investigations have shed light upon the catalytic roles of noble metal nanoparticles as active sites in selective oxidation of alcohols due to their superior catalytic performance compared to non-noble metals [1]. Since the first successful report regarding the Pd-catalyzed oxidation of secondary alcohol, numerous results have been reported on the Pd catalysts and their catalytic applications in alcohol oxidation. Mori et al. reported that Pd supported on hydroxyapatite (Pd/HAP) possessed a turnover frequency (TOF) of 9800 h^{-1} for 1-phenylethanol oxidation under mild conditions in the absence of solvent [2]. The zeolite-supported Pd catalysts exhibiting an extraordinarily high TOF of 18,800 h^{-1} for 1-phenylethanol oxidation has also been reported by Li et al. [3].

The dispersion and size distribution of metal nanoparticles make significant difference on the catalytic behavior in certain reactions, such as alcohol oxidation which is generally considered as a size-dependent reaction [4]. Usually, highly dispersed metal nanoparticles with narrow size distribution exhibit excellent catalytic activity due to the specific electronic structure and high fractions of the coordination unsaturated metal atoms [5–9].

For instance, the metal particle size plays a major role in controlling catalytic activity in CO oxidation, and the activity increases remarkably when Au diameter decreases to 5 nm [10–14]. Fang et al. reported the sharp increase of TOF for benzyl alcohol dehydrogenation when the average Au particle size decreases from 4 nm to 2.1 nm. It was suggested that the Au nanoparticles activate substrate over the low-coordination surface atoms including the edge and corner sites [5]. Chen et al. also demonstrated that small Pd nanoparticles promoted both the catalytic activity and the selectivity toward benzaldehyde in aerobic oxidation of benzyl alcohol using both experimental and multivariate statistical modeling analysis [15].

Surface property has been proven to be important to control the conversion of substrate and selectivity toward the desired product. A large number of reports suggested that dehydration of primary or secondary alcohol was catalyzed by acid sites whereas the dehydrogenation to form aldehyde or ketone was catalyzed by both acid and basic [16–20]. Fang and co-authors reported that the Au nanoparticles supported on hydrotalcite, containing both strong surface acidity and basicity, afforded the best catalytic performance among various types of supports screened in dehydrogenation of benzyl alcohol. They speculated a mechanism with the base cleaving the O—H bond of alcohol to form alkoxide intermediate while acid sites participating in metal hydride to yield H$_2$ [5]. Base is usually applied as a promoter into the catalyst for oxidation of alcohols [21,22]. Wang et al. reported that surface basicity favored both conversion of benzyl alcohol and selectivity toward benzaldehyde while surface acidity promotes the conversion of benzyl alcohol at

---

* Corresponding author. Tel.: +65 6316 8940; fax: +65 6794 7553.
  E-mail addresses: yhyang@ntu.edu.sg, yanhui.yang@live.com (Y. Yang).

the expense of selectivity due to the formation of a large amount of byproducts, such as dibenzyl ether and hydrobenzoin [23].

Surface-functionalization is a facile approach to control the surface chemistry of catalyst support and subsequently fine-tune the metal dispersions and metal–support interactions of catalysts. The post-synthesis grafting of functional groups is employed as an alternative to the doping of metal oxides, hydroxide and carbonate. Chen et al. suggested that certain surface organic groups can selectively modify the surface chemistry and hydrophobicity of silica support, thus control the size of metal nanoparticles, dramatically elevated the palladium catalytic performance for benzyl alcohol oxidation [15]. La Parola et al. reported the mercaptopropyl-functionalization of mesoporous silica with enhanced dispersion of metal nanoparticles and metal–support interactions, which further promoted the catalytic activity in the hydrodesulphurization [24]. The immobilized functional groups (e.g., –NH$_2$ and –SH) anchor and stabilize metal nanoparticles. The localized basicity on surface-functionalized support enhanced the activation of benzyl alcohol in aerobic dehydrogenation, reduced the extent of side reactions, and accelerated the desorption of intermediate products [25]. Moreover, the surface functional groups may contribute to the variation in the electron density and conductivity of carbon nanotube (CNT) supports [26].

CNT has attracted tremendous attention as a catalyst support material due to its mechanical properties, electrical conductivity and thermal stability. The high accessibility of active phase remarkably eliminates mass diffusion resistance and intra-particle mass transfer problem in reaction medium [27]. Zhou et al. reported the Pt alloyed with Fe catalysts supported on CNT for aerobic oxidation of benzyl alcohol in aqueous phase [28]. A high catalytic activity (TOF of 19,467 h^{-1}) of Pd nanoparticles supported on manganese oxide-doped CNT has also been reported by Tan et al. [29]. In this study, it is aimed to synthesize and investigate the Pd nanoparticles supported on CNT surfaces functionalized by organosilane modifiers, especially amino-containing groups. The as-prepared catalysts were evaluated in the aerobic oxidation of benzyl alcohol in the absence of solvent as a model reaction. Furthermore, correlation between surface chemistry, catalyst structure, electrochemical activity, and catalytic performance was discussed in depth.

2. Experimental

2.1. Catalyst synthesis

CNT (>95%, Cnano) was pre-treated with concentrated nitric acid to remove the metallic impurities as well as the amorphous carbon following the processes described by Lordi et al. [30]. Abundant surface functional groups were created during the pretreatment, which served as anchoring sites for further post-synthesis grafting of organosilane functionalities. Organosilanes, i.e., (3-aminopropyl) triethoxysilane (APS, ≥98%, Sigma–Aldrich), hexamethyldisilazane (HMDS, Sigma), and [3-(2-aminoethylamino) propyl] trimethoxysilane (ATMS, 97%, Aldrich) were linked onto CNT surfaces via a post-synthesis grafting method shown in Scheme 1. A typical preparation procedure, using APS-functionalized CNT as an example is as following. 1.0 g of CNT was suspended in 30 mL of toluene and refluxed for 12 h at 110 °C under nitrogen flow (50 mL min^{-1}), followed by adding 2.4 mmol of APS (or a certain amount of other silane modifiers) and stirring continuously for 5 h. After filtering the mixture, the resulting powder was washed with toluene, and dried at 80 °C. The samples were correspondingly denoted as APS-CNT, HMDS-CNT, and ATMS-CNT.

Palladium nanoparticles supported on surface-functionalized CNT were prepared by adsorption–reduction method

[31]. Mixture of 375.9 μL of 0.05 M PdCl$_2$ aqueous solution and 0.2 g of surface-functionalized CNT, e.g., APS-CNT, were suspended in 20 mL of deionized water, followed by stirring for 5 h at 80 °C. The resulting powders were filtered, washed with deionized water, and dried at 80 °C overnight. The catalysts were reduced at 400 °C under H$_2$ flow of 20 mL min^{-1} for 2 h and correspondingly denoted as 1Pd/APS-CNT, where 1 indicates the 1 wt.% of Pd loading.

2.2. Catalyst characterizations

Powder X-ray diffraction (XRD) patterns were recorded on Bruker AXS D8 diffractometer with filtered Cu Kα radiation (λ = 0.15406 nm) at 40 kV and 40 mA under ambient condition. Diffraction data were collected between 10° and 80° (2θ) with a resolution of 0.02° (2θ). Transmission electron microscopy (TEM) was carried out on a JEOL JEM-2100F at 200 kV. The samples were dispersed in ethanol and dropped on carbon coated holey Cu grids. Metal contents were detected by inductively coupled plasma (ICP). Nitric acid was employed to dissolve the sample. The pH value of CNT and different organosilanes functionalized CNT supports were measured following methods reported by Tian et al. [32]. 0.2 mg of sample was dispersed in 10 mL of boiling distilled water, cooled to room temperature and stirred overnight to reach balance. After filtration of the suspension, the pH value of the filtrate was measured by a pH meter. X-ray photoelectron spectroscopy (XPS) measurement was carried out on VG Escalab 250 spectrometer with Al Kα 1846.6 eV anode. C 1s peak at 284.6 eV was employed as the reference for calibration of binding energy.

Raman spectra were performed on a Renishaw Raman spectrometer under an Ar excitation laser light 514.5 nm, of which the detection depth is about 150 nm. UV–vis–NIR diffusive reflectance spectra were recorded on a Varian-Cary 5000 UV–vis–NIR spectrophotometer equipped with diffuse reflectance accessories. The spectra were collected in the range of 1700–2600 nm at room temperature with BaSO$_4$ as reference. Samples were dried overnight at 80 °C prior to the test.

Cyclic voltammetry (CV) and CO stripping voltammetry were conducted in 1.0 M KOH aqueous solution at the rate of 50 mV s^{-1} (Princeton Applied Research, Versa STAT 3 Potentiostat/Galvanostat). Catalyst ink was prepared by dispersing 2 mg of catalyst into 3 mL of 0.025 wt.% Nafion in ethanol solution ultrasonically. The working electrode was prepared by dropping 30 μL of ink onto a glassy carbon electrode within the carbon area. Hg/HgO (1.0 M KOH) electrode and Pt foil were employed as reference and counter electrodes, respectively. Potential range of CV measurement was controlled between −0.8 and 0.3 V. CO stripping was carried out in the following procedures: after purging nitrogen into KOH aqueous solution for 20 min, CO was purged for another 15 min to generate CO layer on the catalyst surfaces meanwhile the potential was kept at −0.8 V. Potential of CO stripping voltammetry was also ranged between −0.8 and 0.3 V.

2.3. Aerobic oxidation of benzyl alcohol

The catalytic reaction employed solvent-free oxidation of benzyl alcohol with molecular oxygen in a bath-type reactor under the atmospheric pressure. 50 mmol of benzyl alcohol (5.174 mL) was added into a three-necked glass flask pre-charged with 0.01 g of catalyst (benzyl alcohol/Pd = 500 mol/g). The flask was immersed in a silicone oil bath at 160 °C with the oxygen flow rate of 20 mL min^{-1} to initiate the reaction. The reaction ran for 1 h under vigorous stirring at the speed of 1200 rpm. After the reaction, the solid catalyst was filtrated and the liquid phase was analyzed by an Agilent gas chromatography 6890 armed with HP-5 capillary column. Dodecane was the internal standard to quantify the percentage
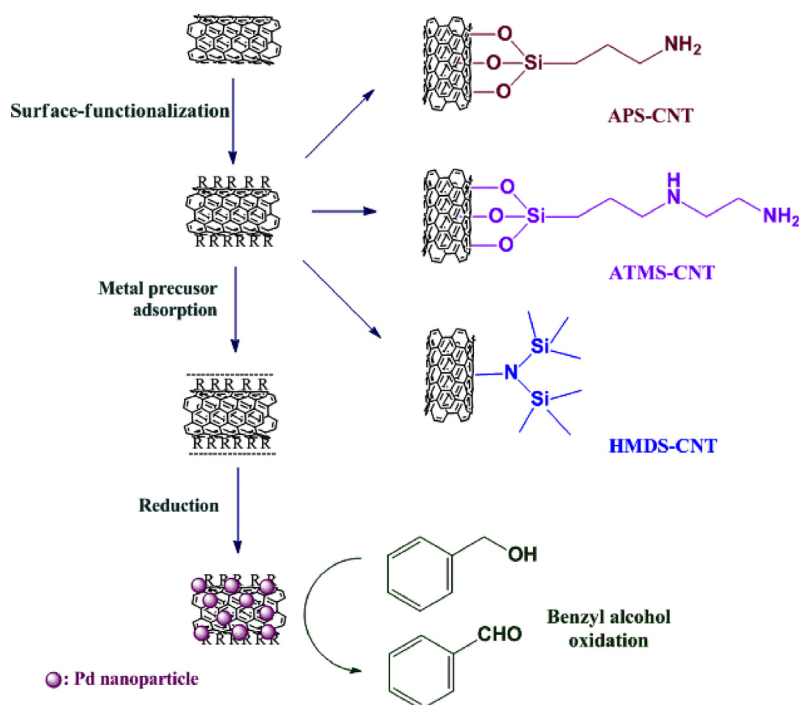
Scheme 1. Preparation process and catalytic evaluation of surface-functionalized CNT supported Pd catalysts.

of residual reactant and products in order to evaluate benzyl alcohol conversion and benzaldehyde selectivity [33]. The definition of conversion, selectivity, turnover frequency (TOF) and quasi-turnover frequency (qTOF) are as follows [15,34], where the electro-active surface area was measured by CO stripping voltammetry [34]:

$$\text{Conversion}(\%) = \frac{\text{moles of reactant converted}}{\text{moles of reactant in feed}} \times 100\%$$

$$\text{Selectivity}(\%) = \frac{\text{moles of product formed}}{\text{moles of reactant converted}} \times 100\%$$

$$\text{qTOF}(h^{-1}) = \frac{\text{moles of reactant converted}}{\text{moles of Pd} \times \text{dispersion} \times \text{reaction time}(h)}$$

$$\text{Dispersion} = \frac{\text{Electroactive surface area}}{(1/\text{atomic weight of Pd})) \times (N_A \times 4\pi r_{Pd}^2)}$$

3. Results and discussion

3.1. Effect of organosilane functional groups

The surface chemistry, which is reflected from the pH in this study, has a crucial role in Pd nanoparticle sizes, size distributions, and metal–support interaction. Table 1 shows the pH measurements of 1Pd/CNT and surface-functionalized CNT supported catalyst. A distinct variation in pH is observed with different surface functionalities. The surface of nitric acid pretreated CNT is mildly acidic, with a pH of 6.2. APS and ATMS surface functionalized CNT possess increased pH of 9.1 and 9.8, respectively, indicating that amino-containing functional groups are able to enhance the basicity of CNT surfaces. HMDS-functionalized CNT shows a neutral surface as anticipated. The pH variations substantiate the successful functionalization with surface groups and the effective tuning of the surface basicity.

Xu et al. suggested that adsorption bands of well-isolated amino groups and hydroxyl groups cannot be resolved using FTIR due to the overlap of bending vibration between NH and OH groups in
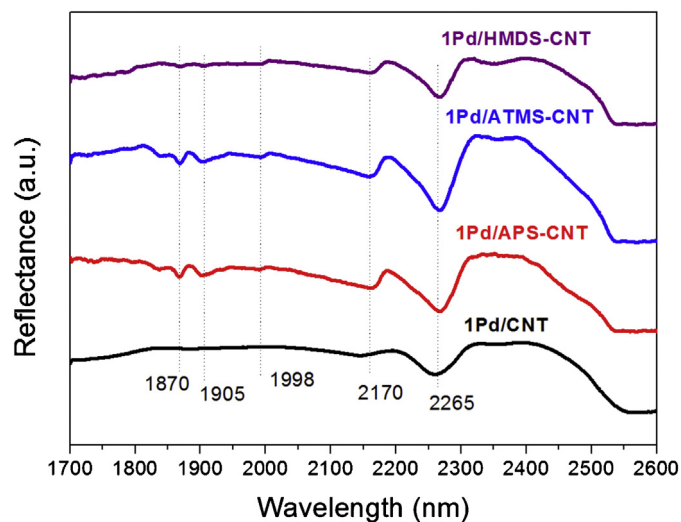

Fig. 1. The UV–vis–NIR spectra of 1Pd/CNT, 1Pd/APS-CNT, 1Pd/ATMS-CNT and 1Pd/HMDS-CNT.

IR range [35]. Near-infrared (NIR), on the other hand, is able to characterize amino groups since amino groups exhibit well-resolved bands in the region between 1000 and 2500 nm, i.e., NIR region. As shown in Fig. 1, palladium supported on hydrophilic APS- and ATMS-functionalized CNT samples demonstrate two major reflection bands: 1870 nm and 1905 nm indexed to the stretching and deformation vibrations for adsorbed water molecules [36], which are hardly discernible for relatively more hydrophobic 1Pd/CNT and 1Pd/HMDS-CNT samples. The reflection band at 1998 nm is assignable to the combination of stretching (ν) and bending (δ) vibrations of the amino groups [15,37], which cannot be observed in 1Pd/CNT catalyst due to the lack of amino groups. The reflection bands at 2170 and 2265 nm are identified to the infrared optical response of CNT when the electron charge transition from valence band to conduction band ($V_i \rightarrow C_i$) upon the

Table 1
pH and Catalytic results of benzyl alcohol oxidation over 1Pd/CNT, 1Pd/APS-CNT, 1Pd/ATMS-CNT and 1Pd/HMDS-CNT catalysts.[a]
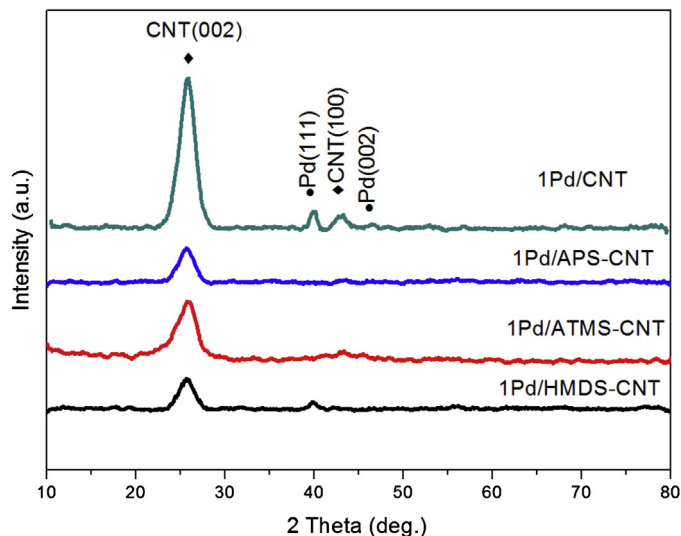
Catalyst	pH	Pd[b] (wt.%)	EAS[c] ($m^2 g^{-1}$)	Conversion (%)	Selectivity (%)			qTOF[d] (h^{-1})
					Benzaldehyde	Toluene	Benzoic acid	
1Pd/CNT	6.2	0.96	12.1	17.1	95.3	2.1	2.6	177,483
1Pd/APS-CNT	9.1	0.98	14.3	27.8	91.9	1.2	6.9	288,755
1Pd/ATMS-CNT	9.8	0.97	14.8	19.9	95.1	1.9	3.0	184,208
1Pd/HMDS-CNT	7.3	0.93	11.9	12.8	97.6	0.8	1.6	125,089

[a] Reaction conditions: catalyst, 10 mg (the amount of Pd is 1 wt.% of catalyst, 0.1 mg); benzyl alcohol, 50 mmol; O_2, 20 mL min^{-1}; temperature, 160 °C; time, 1 h.

[b] Metal content was obtained by ICP.

[c] EAS areas were measured from CO stripping data.

[d] qTOF is defined as the number of benzyl alcohol molecules converted in 1 h on one active site; the number of active sites (Pd atoms exposed on the surface) is determined by EAS value [51] considering Pd content obtained from ICP, and subtracted the CNT effect (conversion ~5%).
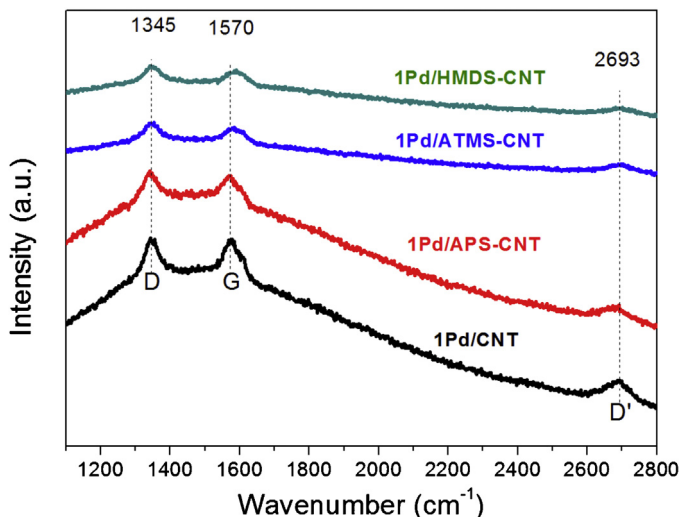
Fig. 2. Raman spectra of 1Pd/CNT, 1Pd/APS-CNT, 1Pd/ATMS-CNT and 1Pd/HMDS-CNT.

Fig. 3. XRD patterns of 1Pd/CNT, 1Pd/APS-CNT, 1Pd/ATMS-CNT and 1Pd/HMDS-CNT.

photon absorption at 0.573 and 0.548 eV, respectively [38,39]. Due to the characteristic infrared optical response of CNT support, all the samples possess evident peaks at 2170 and 2265 nm, whereas an noticeable increase of charge transfer strength occurs when functional groups (i.e., APS, ATMS and HMDS) are grafted onto the CNT surface, indicating that these functional groups can elevate the electron density on CNT surface, thus increase the number of electrons undergoing the transition from valence band to conduction band. The UV–vis–NIR characterization further verified that after surface functionalization, the CNT surfaces are indeed grafted with functional groups and these functional groups have an impact on the surface electron density of CNT support.

Raman spectroscopy was employed to characterize the CNT supports and the results are shown in Fig. 2. The characteristic G-band, situated at 1570 cm^{-1}, is derived by the graphite-oriented Raman-active E_{2g} mode [40,41]. Amorphous carbon-oriented D-band is centered at 1345 cm^{-1} and the second-order harmonic D′-band is indexed at 2693 cm^{-1} due to the finite size effect, lattice distortion, and the structural defect [42]. The slight decrease in the G-, D- and D′-band intensities implies the less perfect structure of the nanotubes after surface-functionalization with various organosilane modifiers [41]. The ratio of G to D band peak intensity (I_G/I_D) of 1Pd/CNT, 1Pd/APS-CNT, 1Pd/ATMS-CNT and 1Pd/HMDS-CNT have been measured and the results are 1.80, 1.48, 1.53, and 1.33, respectively. The decrease of I_G/I_D after surface-functionalization indicates the decline of CNT purity to certain extent upon post-synthesis grafting organic groups [42].

XRD patterns and TEM images were employed to characterize the Pd nanoparticles supported on organosilane modified CNT

surfaces. XRD patterns of catalysts with Pd loading of 1 wt.% are displayed in Fig. 3. The XRD peaks at 26.01° and 42.80° are attributed to the (0 0 2) and (1 0 0) facets of CNT, respectively [29]. For 1Pd/CNT and 1Pd/HMDS-CNT, the diffraction peak at 40.00° is in correspondence with the (1 1 1) facet of palladium face-centered cubic (FCC) crystalline structure. The larger full width at half maximum (FWHM) value of this particular diffraction peak of 1Pd/HMDS-CNT indicates that 1Pd/HMDS-CNT possesses smaller Pd average size than 1Pd/CNT according to Scherrer equation [43,44]. Diffraction peaks indexed to Pd FCC structure are indiscernible for 1Pd/APS-CNT and 1Pd/ATMS-CNT, implying the highly dispersed nature of Pd nanoparticles and the particle sizes are below the detection limit of XRD.

The higher dispersion and smaller mean size of Pd nanoparticles have been achieved after functionalizing CNT surfaces with organosilane modifiers; these results can be further verified through TEM observations and the results are illustrated in Fig. 4. 1Pd/CNT presents a wide Pd particle size distribution scattered around 6 nm. 1Pd/APS-CNT and 1Pd/ATMS-CNT demonstrate narrow palladium nanoparticle size distributions centered at 2.1 nm and 3.9 nm, respectively. 1Pd/HMDS-CNT exhibits a broad size distribution with an average particle size of 6.5 nm. Upon CNT surface-functionalization with organosilanes, these groups serve as anchoring sites for metal adsorption. Hydrophilic amino groups are highly affinitive to aqueous palladium ions, hence favor the deposition of metal precursors, which leads to highly dispersed palladium nanoparticles supported on CNT surfaces. Moreover, the basic –NH$_2$ and –NH– groups undergo a hydrolysis, resulting in the positively charged surfaces, which consequently shows great
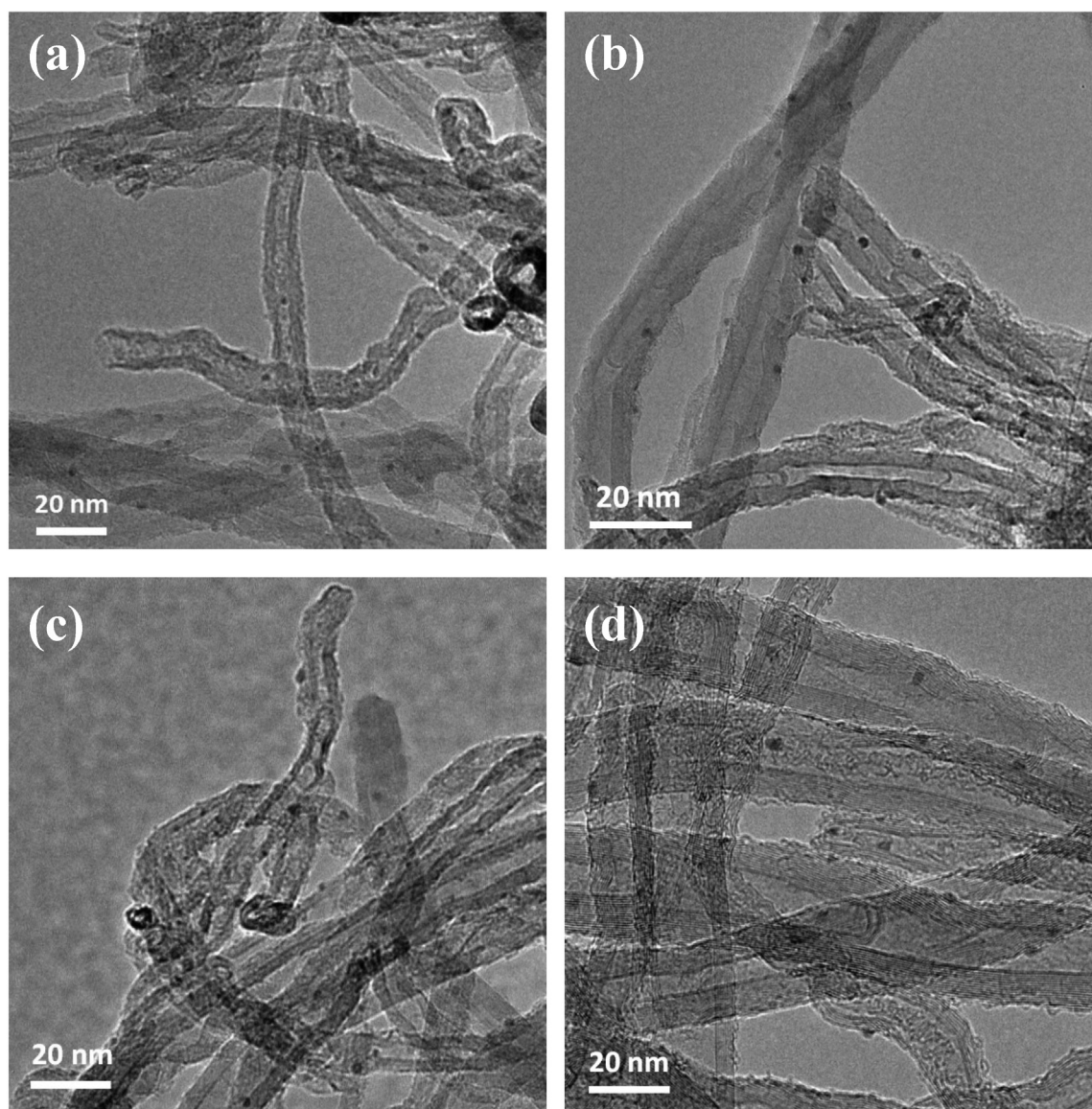
Fig. 4. TEM images and particle size distribution histograms of 1 wt.% palladium supported on CNT functionalized with different functional groups: (a) 1Pd/CNT; (b) 1Pd/APS-CNT; (c) 1Pd/ATMS-CNT; (d) 1Pd/HMDS-CNT.

affinity to $PdCl_2(OH)_2^{2-}$ precursors. The hydrophobic trimethyl groups show adsorption barrier for palladium precursors, thus lead to large Pd particle size with a broad size distribution. Furthermore, 1Pd/APS-CNT possesses a smaller palladium nanoparticle mean size and a narrower size distribution than 1Pd/ATMS-CNT. Similar results ascribed to strong interaction between Pd nanoparticles and the grafted diamino functional groups were also reported by Lee et al. [45].

The Pd 3d and O 1s XPS core level spectra were investigated and deconvoluted as shown in Fig. 5. The Pd 3d peaks were convoluted to two oxidation states due to the coexistence of Pd^0 metallic state and Pd^{2+} cationic state. The fractions of Pd^0 (Pd^0/Pd) in Pd/CNT and Pd/APS-CNT catalysts are 42.3% and 51.7% respectively, implying that the APS functional groups on CNT surface can enhance the electron density of Pd nanoparticles which is associated with the increased CNT electron density after functionalization with APS groups, in agreement with the NIR measurement. The shift of Pd^{2+} $3d_{3/2}$ and $3d_{5/2}$ binding energy peaks toward reduced forms after APS-functionalization implies the presence of Pd in a lower oxidation state or the formation of Pd-APS complex [46]. Since APS contains C—O bonds, the apparent increase of C—O/C=O fraction of

Pd/APS-CNT compared to Pd/CNT indicates the successful functionalization of APS groups onto CNT surface [29].

Cyclic voltammetry (CV) measurements were carried out to characterize their electrochemical properties as shown in Fig. 6. With the organic groups surface-functionalized upon CNT, remarkable increase is observed in the area enclosed by CV curves, which is in correspondence with the results reported by Guo et al. that a larger amount of redox active sites or electron donor sites on CNT surfaces gave rise to a higher capacitance and a larger CV background [47], further verified the NIR results in this study. Upon CNT surface-functionalized with organic groups, i.e., APS, ATMS and HMDS, the palladium oxide (Pd—O) reduction peak shifts from −0.1 to −0.2 V. The Pd—O reduction potential depends on the metal oxide thermodynamics, reduction step kinetics and electrochemical environment [47]. In an alkaline solution, Pd—O reduction mechanism follows the step [48]:

$$PdO + H_2O + 2e^- \rightarrow Pd + 2OH^- \tag{1}$$

The decrease of Pd—O reduction potential when attaching to the functional groups on CNT surfaces indicates that surface organic functional groups covalently σ-bonded on the CNT surface can
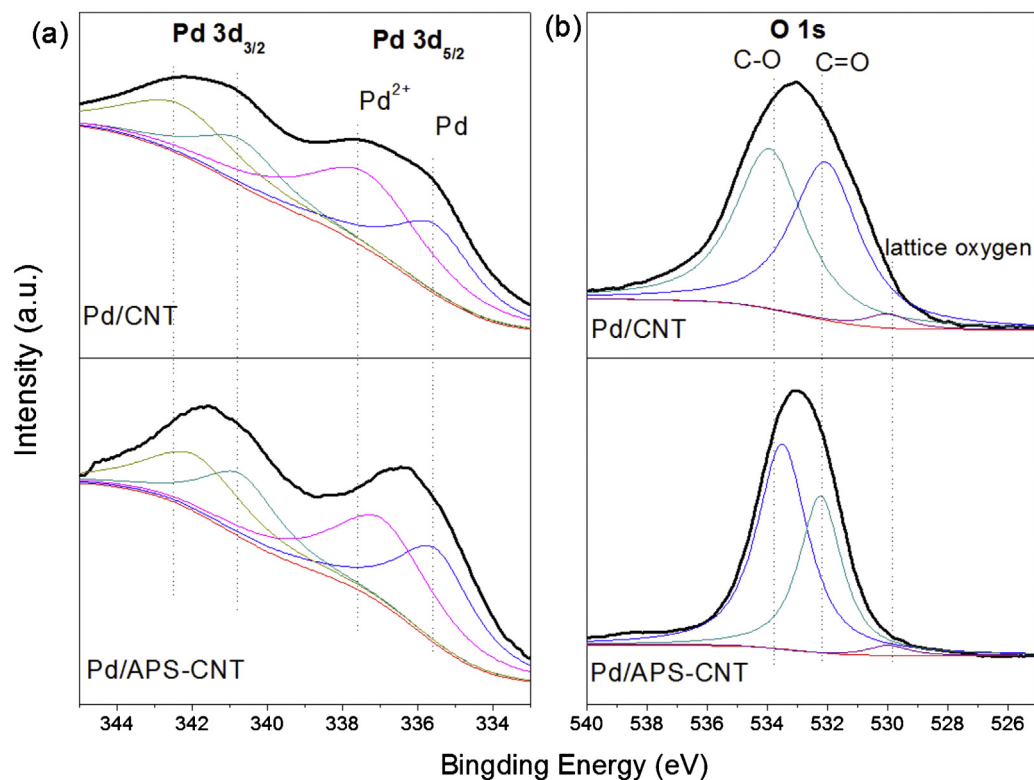
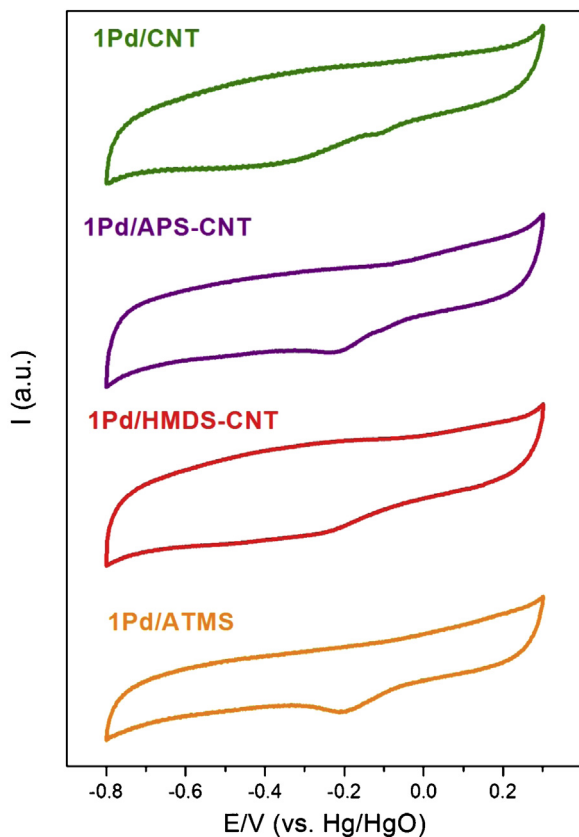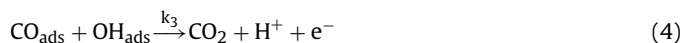**Fig. 5.** XPS spectra: (a) Pd 3d spectra; (b) O 1s spectra.

Fig. 6. Cyclic voltammograms of 1Pd/CNT, 1Pd/APS-CNT, 1Pd/ATMS-CNT and 1Pd/HMDS-CNT.

effectively hinder the Pd—O reduction. Surface-functionalization with organic groups increases the hydrophobicity of CNT surface, which hampers the contact between water and CNT support, resulting in a difficulty of Pd—O reduction. Although amino-containing groups contribute a higher conductivity of CNT, which enhances the electric current in response to the electric potential applied and accelerates the electron diffusion to Pd particles, the water approachability to CNT plays a more crucial role in this particular Pd—O reduction step.

CO stripping voltammetry is carried out to measure the electrochemical active surface (EAS) areas of Pd nanoparticles. CO molecules adsorbed on Pd nanoparticles are subsequently oxidized to CO_2 at a negative onset potential, followed by the positively sweeping potential on the working electrode. The commonly accepted model for CO electro-oxidation is the Langmuir–Hinshelwood mechanism, where adsorbed OH formed on the Pd surfaces by dissociative adsorption of H_2O reacts with the adsorbed CO [49].

$$H_2O_{ads} \xrightarrow{k_1} OH_{ads} + H^+ + e^- \tag{2}$$

$$OH_{ads} + H^+ + e^- \xrightarrow{k_2} H_2O_{ads} \tag{3}$$

$$CO_{ads} + OH_{ads} \xrightarrow{k_3} CO_2 + H^+ + e^- \tag{4}$$

The electrolyte KOH aqueous solution neutralizes the H^+ and promotes the reaction moving forward. Thus, CO electro-oxidation potential relies upon the kinetics, thermodynamics, and electrochemical environment of CO molecules, as well as the electrochemical state of Pd. As displayed in Fig. 7, CO electro-oxidation peak splits into multiple peaks when CNT support is surface-functionalized with organic groups. it is postulated that the CNT surfaces are not homogeneous even after modifying with organic groups, i.e., Pd nanoparticles may be directly in contact with organic groups, bare CNT surfaces, and bareCNT surfaces in
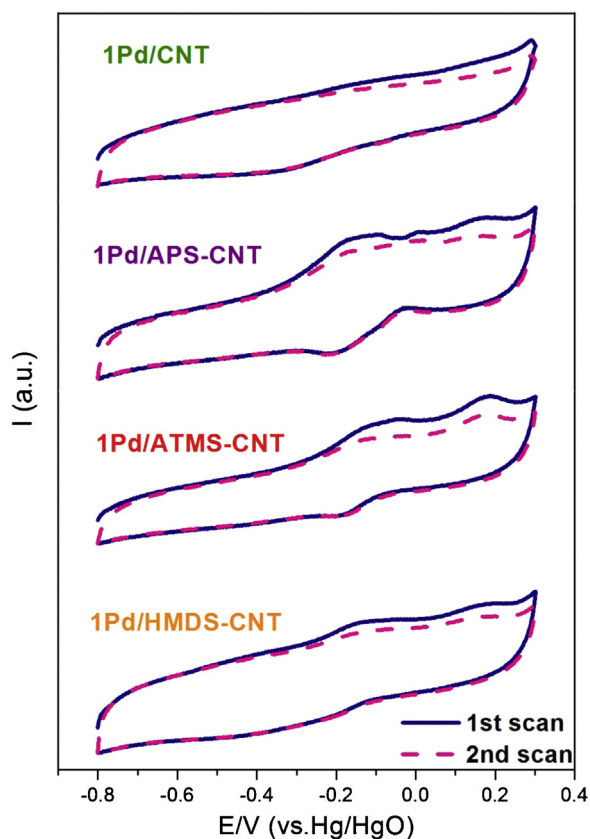
Fig. 7. CO stripping voltammograms of 1Pd/CNT, 1Pd/APS-CNT, 1Pd/ATMS-CNT and 1Pd/HMDS-CNT.

the vicinity of organic modifiers (or vice versa). Pd nanoparticles may possess different electron densities if they are anchored at different sites due to the electronic interaction between Pd nanoparticles and CNT surface substrates. Subsequently, CO molecules adsorbed on these Pd nanoparticles may show different adsorption strength, resulting in the variation of electro-oxidation potentials. The CNT surface free energy may also be different in the presence or absence of organic modifiers, which significantly impact the kinetics rate constant k_1, k_2, and k_3 of the Langmuir–Hinshelwood mechanism. Additionally, the dynamic adsorption and desorption of CO from surface-functional groups, which possibly disturbs the CO oxidation potential on Pd surface, also contribute to the split of CO electro-oxidation peaks. The EAS areas of Pd nanoparticles have been calculated based upon the CO stripping voltammetry, with the assumption that the oxidation of a CO full monolayer adsorbed on Pd surfaces requires 420 μC/cm^2 of electric charge [50]. The results in Table 1 show the larger electro-chemical active surface area of Pd on APS and ATMS functionalized CNT support than Pd on bare CNT surfaces due to the smaller particle sizes of 1Pd/APS-CNT and 1Pd/ATMS-CNT catalysts. Pd on HMDS-functionalized CNT possesses the lowest EAS area because of the large Pd particle size.

Solvent-free selective oxidation of benzyl alcohol with molecular oxygen was introduced as a probe reaction to shed light on the effect of surface functionalization on catalytic performance of Pd nanoparticles, and the results are displayed in Table 1. qTOF was defined as the number of benzyl alcohol molecules converted in 1 h on one active site determined by EAS measurements [51]. The main product is benzaldehyde and byproducts are a trace amount of toluene and benzoic acid. The catalytic activity is enhanced after functionalizing the CNT surfaces with APS and ATMS. 1Pd/APS-CNT displays the best catalytic activity with the
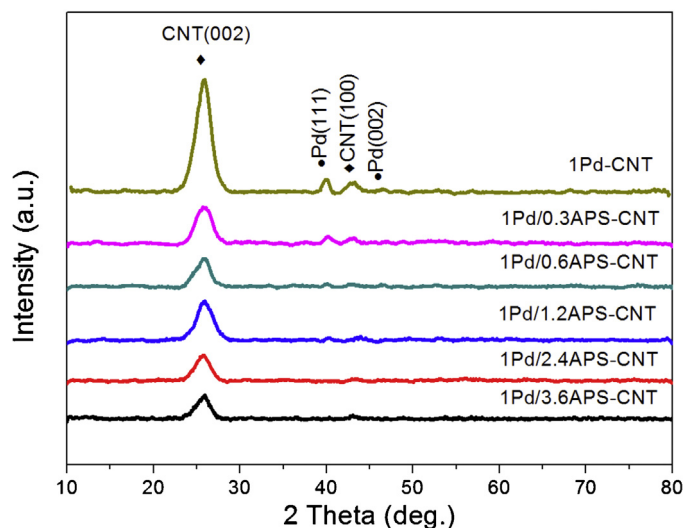

Fig. 8. XRD pattern of 1Pd/APS-CNT with different APS amount.

conversion of 27.8%, and the qTOF of 288,755 h^{-1}, which are 1.6 times higher than those of 1Pd/CNT. Nonetheless, the high activity is at the expense of the slightly decreased selectivity toward benzaldehyde (91.9%). 1Pd/HMDS-CNT shows the lowest catalytic activity with the conversion of 12.8% and the qTOF of 125,089 h^{-1}. Nevertheless, the highest selectivity toward benzaldehyde (97.6%), as well as the lowest selectivity to byproducts toluene (0.8%) and benzoic acid (1.6%).

Benzyl alcohol dehydrogenation forms benzaldehyde and co-product H$_2$ in the absence of O$_2$. C—O bond hydrogenolysis of benzyl alcohol also occurs to form toluene when Pd is in metallic state (Pd^0) partially covered with hydrogen yielded from the benzyl alcohol dehydrogenation of even in the presence of molecular oxygen [52].

$$PhCH_2OH \rightarrow PhCHO + H_2 \tag{5}$$

$$PhCH_2OH + H_2 \rightarrow PhCH_3 + H_2O \tag{6}$$

Although molecular oxygen is a good acceptor for hydrogen, toluene is inevitable due to benzyl alcohol. The direct insertion of oxygen into benzyl alcohol is slow [53] and surface water is formed as a co-product. Benzoic acid is then formed by hydration of benzaldehyde to a germinal diol and subsequently undergoes the dehydrogenation reaction on Pd [52].

$$PhCHO_{ad} + H_2O_{ad} \rightarrow PhCH(OH)_{2,ad} \tag{7}$$

$$PhCH(OH)_{2,ad} \rightarrow PhCOOH_{ad} + 2H_{ad} \tag{8}$$
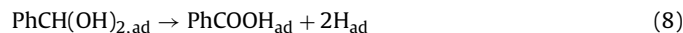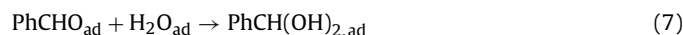
Additionally, basic sites of catalysts promote the disproportionation of benzaldehyde (i.e., the Cannizzaro reaction), forming benzoic acid and benzyl alcohol [54], which is employed to explain the effect that the –NH$_2$ containing APS and ATMS surface-functionalized catalysts produce more benzoic acid than 1Pd/CNT and methyl-covered 1Pd/HMDS-CNT catalysts.

$$2PhCHO + H_2O \xrightarrow{base} PhCH_2O + PhCOOH \tag{9}$$

Thus, the higher selectivity to benzaldehyde is ascribed to the same effect that low surface hydrogen concentration leads to diminished formation of toluene and the low surface basicity results in little extent of disproportionation of benzaldehyde to form benzoic acid.

In addition, the basic catalyst support facilitates small and highly dispersed Pd nanoparticles with narrow size distribution. Referring to the TEM results in Fig. 4, Pd nanoparticles average sized 2 nm with a narrow size distribution on 1Pd/APS-CNT can explain the remarkably high activity of this particular catalyst, considering
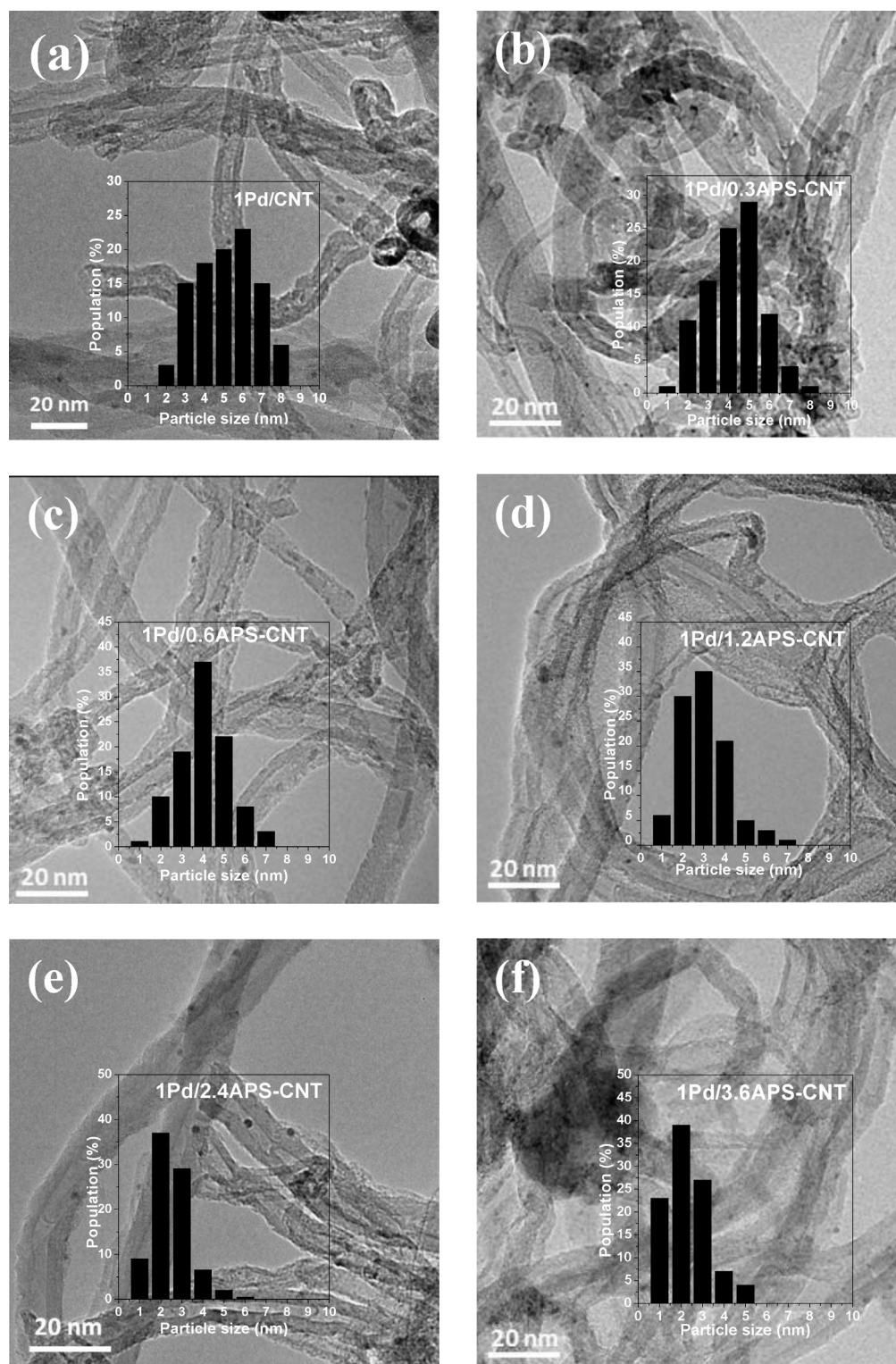
Fig. 9. TEM graphs and Pd particle size distribution of (a) 1Pd/CNT; (b) 1Pd/0.3APS-CNT; (c) 1Pd/0.6APS-CNT; (d) 1Pd/1.2APS-CNT; (e) 1Pd/2.4APS-CNT; (f) 1Pd/3.6APS-CNT.

the vital role that Pd nanoparticle size plays in this size-dependent reaction, which is in agreement with results reported by Chen et al. [15]. The basic amino group-functionalized catalysts possess surface basicity which is suggested to facilitate the alcohol adsorption and product desorption from the Pd active sites. Although both APS and ATMS contain amino groups, diamine groups in ATMS have stronger interaction with Pd nanoparticles which hampers the exposure of Pd active sites than that of monoamine in APS, hence

1Pd/APS-CNT displays a more remarkable enhancement in catalytic activity. The low Pd content in 1Pd/HMDS-CNT is attributed to the adsorption barrier caused by the hydrophobic tri-methyl groups attached surface when palladium is adsorbed onto it. According to the TEM result in Fig. 4, this adsorption barrier also results in large Pd nanoparticle size with a broad size distribution. This particular catalyst shows the lowest benzyl alcohol conversion (12.8%), which can be explained by the lack of active sites owing to the low

Pd content, and the large Pd particle sizes indexed in XRD and TEM. Considering the excellent yield for benzaldehyde, APS was selected as the best modifier in the following study.

3.2. Effect of APS content

The XRD patterns of 1Pd/APS-CNT catalysts functionalized with different APS loadings are shown in Fig. 8. There is an obvious decreasing of diffraction peak intensity at 40.00°, the Pd characteristic (1 1 1) facet, and a discernible increase of FWHM of the 40.00° peak with increasing the amount of functionalized APS groups. According to the Debye–Scherrer equation [43,44], the average size of Pd nanoparticles decreases with the increase in FWHM, and hence the increasing APS loading facilitates the Pd dispersion. The Pd characteristic diffraction peaks cannot be observed in 1Pd/2.4APS-CNT and 1Pd/3.6APS-CNT catalysts, implying the Pd nanoparticles are uniform with small sizes beyond the detection of X-ray signals. Chen et al. suggested that the specific metal–support interaction and the distribution of metal nanoparticles are dependent upon the nature of support surface chemistry [15]. After purified through the nitric acid treatment, the CNT surfaces without APS are mildly acidic and negatively charged due to the ionization of carboxyl groups, which hampers the diffusion and adsorption of $PdCl_2(OH)_2^{2-}$ negatively charged precursors. After grafting the terminal APS groups, the hydrolysis of basic –NH$_2$ groups changes the surface to positively charged, showing great affinity to the negatively charged precursors. Additionally, these attached amino groups can act as anchors for the stabilization of Pd nanoparticles through covalent interactions, giving rise to highly dispersed Pd nanoparticles [15,55]. Nonetheless, further adding APS possibly causes the oligomerization and polymerization of organosilanes which forms a cross-linked alkanolamine attached on CNT surfaces [56], making the Pd particles less finely tuned. From the TEM results shown in Fig. 9, 1Pd/CNT possesses the largest Pd nanoparticle size with a wide distribution scattered around 6 nm. Whereas 1Pd/2.4APS-CNT demonstrates the smallest Pd nanoparticle size with a narrow distribution centered at 2.1 nm. As the APS amount increases in the series of 0.3, 0.6, 1.2, 2.4 and 3.6 mmol per gram of CNT, Pd nanoparticle mean size turns out to be 4.5 nm, 3.9 nm, 3.1 nm, 2.1 nm and 2.3 nm respectively. Hence, the TEM observation further corroborates the XRD results that an evident decrease of Pd nanoparticle size occurs with the increase of the amount of APS surface groups.

As mentioned earlier, the pH is able to reflect the surface chemistry, which has a crucial role in Pd nanoparticle sizes and size distributions, metal–support interaction, as well as the catalytic performance in solvent-free selective oxidation of benzyl alcohol. Table 2 displays the pH measurement results of different content of APS surface-functionalized CNT supported catalysts. With the increase of APS loading, there is an increase in pH detected in the sequence of 1Pd/CNT < 1Pd/0.3APS-CNT < 1Pd/0.6APS-CNT < 1Pd/1.2APS-CNT < 1Pd/2.4APS-CNT < 1Pd/3.6APS-CNT, indicating that functionalization with amino-containing functional groups is able to enhance the surface basicity of CNT support. All these pH variations corroborate the successful surface-functionalization with different amount of APS groups and the effective tuning of the catalysts supports surface basicity.

As suggested previously [35], adsorption bands of amino groups and hydroxyl groups cannot be well resolved using FTIR due to the intersection of bending vibration between NH and OH groups within IR range [15]. NIR is superior to FTIR in characterizing amino groups, which can exhibit well-resolved bands in the region between 1000 nm and 2500 nm of wavelength. As shown in Fig. 10, palladium supported on hydrophilic APS functionalized CNT samples possess two major reflection bands: 1870 nm and 1900 nm indexed to the stretching vibration and deformation vibration for
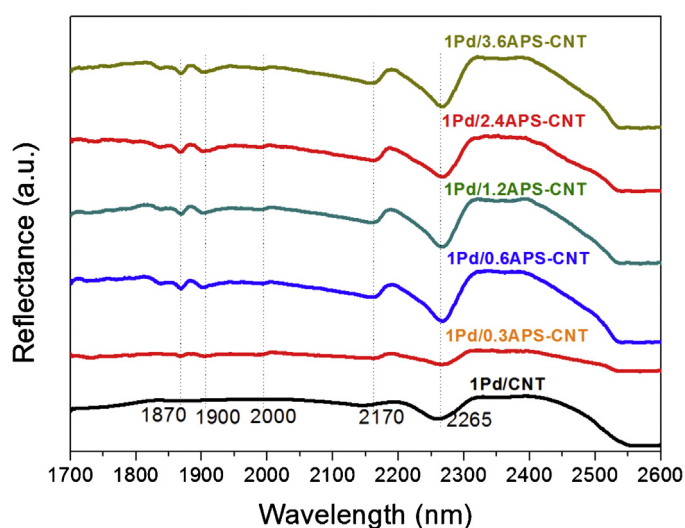

Fig. 10. The NIR spectra of 1Pd/CNT and 1Pd/APS-CNT with different amount of APS.

adsorbed H_2O molecules [36], which cannot be observed for relatively more hydrophobic 1Pd/CNT. The reflection peak at 2000 nm is indexed to the combining stretching vibration (ν) and bending vibration (δ) of the amino groups [15,37], which is hardly visible on 1Pd/CNT without amino-containing surface functional groups. The reflection bands at 2170 nm and 2265 nm are indexed to the near-infrared optical response of CNT when the electron transfer from valence band to conduction band ($V_i \rightarrow C_i$) upon the photon absorption at 0.573 eV and 0.548 eV, respectively [38,39]. When the APS amount is low, the band strength at 2170 nm and 2265 nm is lower than 1Pd/CNT because the nonconductive APS surface functional groups covalently σ-bonded onto CNT surface decrease the π-electron density on CNT and subsequently decreases the number of electrons transferring from valence band to conduction band. With the increase of APS amount, the synergistic effect of the electron-donor induction of the low-electronegativity Si and the APS occupation of CNT electron-withdrawing defect sites (e.g., carboxyl groups, lactone, phenol groups [57]) surpasses the π-electron obstruction effect of APS σ-bonding onto CNT surface, increasing the electron density on CNT support, which leads to enhanced peak strength at 2170 nm and 2265 nm. However, the peak strength at 2170 nm and 2265 nm remains almost unchanged in 1Pd/0.6APS-CNT, 1Pd/1.2APS-CNT, 1Pd/2.4APS-CNT and 1Pd/3.6APS-CNT because the CNT electron-withdrawing defect sites become saturated by the APS surface-functional groups. Therefore, the UV–vis–NIR spectra further indicate that after surface functionalization, the amino-containing APS functional groups have been immobilized onto the CNT surface and these functional groups have modified the nature of CNT surface chemistry.

As shown in Fig. 11, CO stripping voltammograms of catalysts surface-functionalized with different amount of APS groups are recorded. Considering the Langmuir–Hinshelwood mechanism for CO electro-oxidation [49], the kinetics, thermodynamics, and electrochemical environment of CO molecules, as well as the electrochemical state of Pd, determine the electro-oxidation potential of CO molecules. It is obvious that CO electro-oxidation peak splits into multiple peaks when CNT support is surface-functionalized with APS. The peak splits are explained by the difference in CO electro-oxidation potential when it is adsorbed on Pd immobilized on different surface sites (e.g., directly on bare CNT, directly on APS and partially on CNT and APS), resulting in different Pd electron densities and surface free energies. Furthermore, the entrapment and release of CO by the grafted APS groups also contribute to the split of CO electro-oxidation peak considering the

Table 2
pH and Catalytic results of benzyl alcohol oxidation over 1Pd/CNT, 1Pd/0.3APS-CNT, 1Pd/0.6APS-CNT, 1Pd/1.2APS-CNT, 1Pd/2.4APS-CNT and 1Pd/3.6APS-CNT catalysts.[a]

Catalyst	pH	Pd[b] (wt.%)	EAS[c] ($m^2 g^{-1}$)	Conversion (%)	Selectivity (%)			qTOF[d] (h^{-1})
					Benzaldehyde	Toluene	Benzoic acid	
1Pd/CNT	6.2	0.96	12.1	17.1	95.3	2.1	2.6	177,483
1Pd/0.3APS-CNT	7.7	0.94	13.6	7.3	93.9	3.7	2.4	31,931
1Pd/0.6APS-CNT	8.3	0.95	13.8	15.0	96.6	0.4	3.1	135,380
1Pd/1.2APS-CNT	9.0	0.97	14.2	21.4	90.5	5.8	3.7	211,320
1Pd/2.4APS-CNT	9.1	0.98	14.3	27.8	91.9	1.2	6.9	288,755
1Pd/3.6APS-CNT	9.2	1.01	14.5	7.9	96.5	2.5	0.9	35,496

[a] Reaction conditions: catalyst, 10 mg (the amount of Pd is 1 wt.% of catalyst, 0.1 mg); benzyl alcohol, 50 mmol; O_2, 20 mL min^{-1}; temperature, 160 °C; time, 1 h.

[b] Metal content was obtained by ICP.

[c] EAS areas were measured from CO stripping data.

[d] qTOF is defined as the number of benzyl alcohol molecules converted in 1 h on one active site; the number of active sites (Pd atoms exposed on the surface) is determined by EAS value [51] considering Pd content obtained from ICP, and subtracted the CNT effect (conversion ~5%).
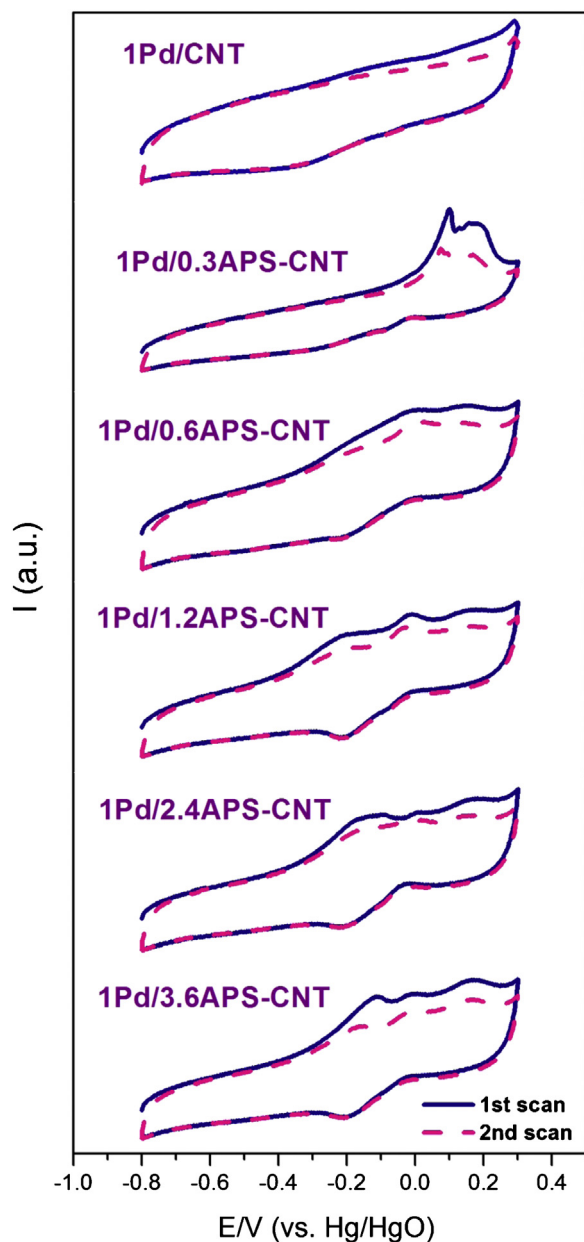

Fig. 11. The CO stripping voltammograms of 1Pd/CNT and 1Pd/APS-CNT with different amount of APS.

perturbation of CO oxidation on Pd surface. As shown in Fig. 11, when the APS amount is low, the clustered CO oxidation main peaks tend to present at higher potential. A small amount of APS covalently σ-bonded to CNT surface hinders the electronic interaction between Pd and CNT support, making the CO electro-oxidation reaction more difficult to proceed. Nevertheless, as the APS amount increases, the cluster of CO oxidation main peaks negatively shifts until 1Pd/2.4APS-CNT, implying that CO molecules can be more easily oxidized on Pd particles with smaller particle size and higher electron densities. However, there is a positive shift of the CO oxidation main peaks cluster from 1Pd/2.4APS-CNT to 1Pd/3.6APS-CNT, which may due to the relatively large Pd nanoparticle of 1Pd/3.6APS-CNT and the excess amount of APS groups. The EAS areas of Pd nanoparticles have been calculated according to the CO stripping voltammetry. As shown in Table 2, the EAS area increases evidently with the increase of APS amount due to the gradually decreased Pd particle sizes, which is in agreement with the XRD and TEM observations. Thus the CO stripping voltammetry further substantiates that appropriate amount of amino-containing APS functional groups can facilitate the formation of highly dispersed small Pd nanoparticles with higher EAS areas. In addition, the negative shift of CO oxidation potentials implies the enhanced catalyst activity for CO electro-oxidation reaction.

Solvent-free benzyl alcohol oxidation over different amount of APS surface-functionalized CNT supported Pd catalysts was investigated and illustrated in Table 2. 1Pd/0.3APS-CNT shows the lowest conversion (7.3%) and qTOF (31,931 h^{-1}), whereas 1Pd/2.4APS-CNT displays the highest conversion (27.8%) and qTOF (288,755 h^{-1}). Low contents of APS covalently σ-bonded onto CNT surface hampers the electron conduction between Pd and CNT support, making the reaction more difficult to proceed, which is in agreement with the CO stripping voltammetry result. Increasing the APS amount evidently increases the catalytic activity until 1Pd/2.4APS-CNT, the most active catalyst in CO electro-oxidation. The sharply decreased conversion and qTOF of 1Pd/3.6APS-CNT are resulted from the decreased Pd particle exposure due to the excess amount of grafted APS groups, which possibly form alkanolamine through oligomerization and polymerization on the CNT support. It can be seen in Table 2, the catalytic performances of these catalysts for aerobic benzyl alcohol oxidation are in accordance with the CO electro-oxidation results. The presence of toluene as the by-product indicates that the Pd nanoparticles are in their reduced state (Pd^0) [52]. Although 1Pd/2.4APS-CNT possesses the highest conversion and qTOF, the selectivity toward benzaldehyde is somewhat unsatisfactory owing to the high selectivity toward benzoic acid.

3.3. Studies on the 1Pd/2.4APS-CNT catalyst

1Pd/2.4APS-CNT, verified to possess the optimal catalytic performance in the solvent-free benzyl alcohol oxidation, has been
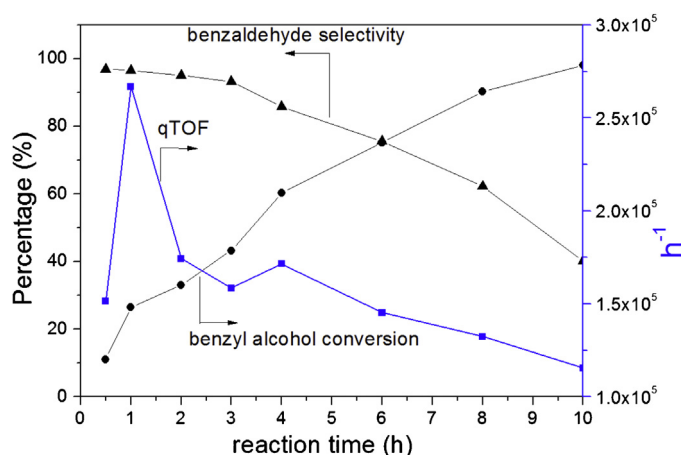
Fig. 12. Time course of 1Pd/2.4APS-CNT for oxidation of benzyl alcohol (reaction condition: benzyl alcohol/Pd = 1000 mol/g; O_2 flow rate = 20 mL min^{-1}; temperature = 160 °C; stirring rate = 1200 rpm).
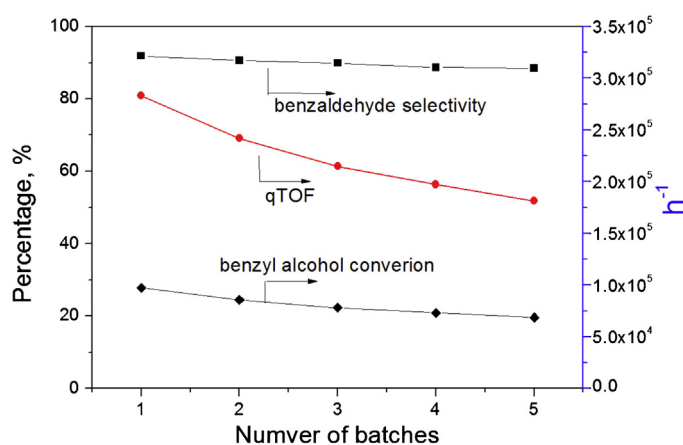

Fig. 13. Recyclability of 1Pd/2.4APS-CNT catalyst for selective solvent free oxidation of benzyl alcohol (reaction conditions: benzyl alcohol/Pd = 1000 mol/g; O_2 flow rate = 20 mL min^{-1}; temperature = 160 °C; reaction time = 1 h; stirring rate = 1200 rpm).

investigated in detail. As depicted in Fig. 12, the time course of 1Pd/2.4APS-CNT for oxidation of benzyl alcohol has been monitored constantly. The benzyl alcohol conversion increases monotonically along with the declined selectivity toward benzaldehyde with the reaction time duration. The qTOF is rather low (151,419 h^{-1}) at the first 0.5 h of reaction; it then rises to 266,845 h^{-1} at 1 h and progressively decreases subsequently. The poor qTOF at the first 0.5 h is possibly due to the reduction of Pd precursors by alcohols, and the gradually decrease of the qTOF after 1 h is ascribed to the diminished amount of reactant benzyl alcohol. The decrease of selectivity toward benzaldehyde is contributed by the further oxidation to form benzoic acid.

The effects of temperature and molecular oxygen flow rate have been investigated and the results are summarized in Table 3. The catalytic activity is not noticeable at low temperature. Furthermore, toluene is formed in a large quantity at low temperature due to benzyl alcohol hydrogenolysis [52]. As the temperature increases, the conversion of benzyl alcohol increases with the decline of selectivity toward toluene, although high temperature favors the deep oxidation of benzaldehyde to form benzoic acid. The activation energy over 1Pd/2.4APS-CNT catalyst is 44.65 kJ/mol. This is similar to that of noble metal catalysts supported on TiO$_2$ reported by Enache et al. (45.8 kJ/mol) [58], but is remarkably higher than the Pd catalyst supported on mesoporous silica SBA-16 material where the reaction is limited by mass diffusion (12.3 kJ/mol) [59,60]. The O_2 flow also shows significant effect on the catalytic performance. Benzyl alcohol can be converted to benzaldehyde by dehydrogenation in the absence of oxygen (conversion 4.7%), along with hydrogen as the co-product. The selectivity toward benzaldehyde is rather low (71.8%) because benzyl alcohol, as the acceptor of hydrogen, undergoes the hydrogenolysis due to the lack of O_2. The conversion increases as the oxygen flow rate is elevated, until the flow rate reaches 20 mL min^{-1}. Then there is an abrupt drop at 30 mL min^{-1} because excess oxygen favors the oxidation of Pd catalyst. With the increase of O_2 flow rate, the selectivity toward toluene is low because oxygen is a good hydrogen acceptor, reducing the coverage of hydrogen on Pd surface and subsequently decreasing the extent of hydrogenolysis which yields toluene.

The recyclability is considered as a crucial factor in evaluating a heterogeneous catalyst in a multiphase system. The active components with poor stability and recyclability leaches out during the reaction course, leading to the formation of active homogeneous catalyst at the cost of losing catalytic activity during consecutive runs. The recyclability of 1Pd/2.4APS-CNT in solvent-free selective oxidation of benzyl alcohol using molecular oxygen has been
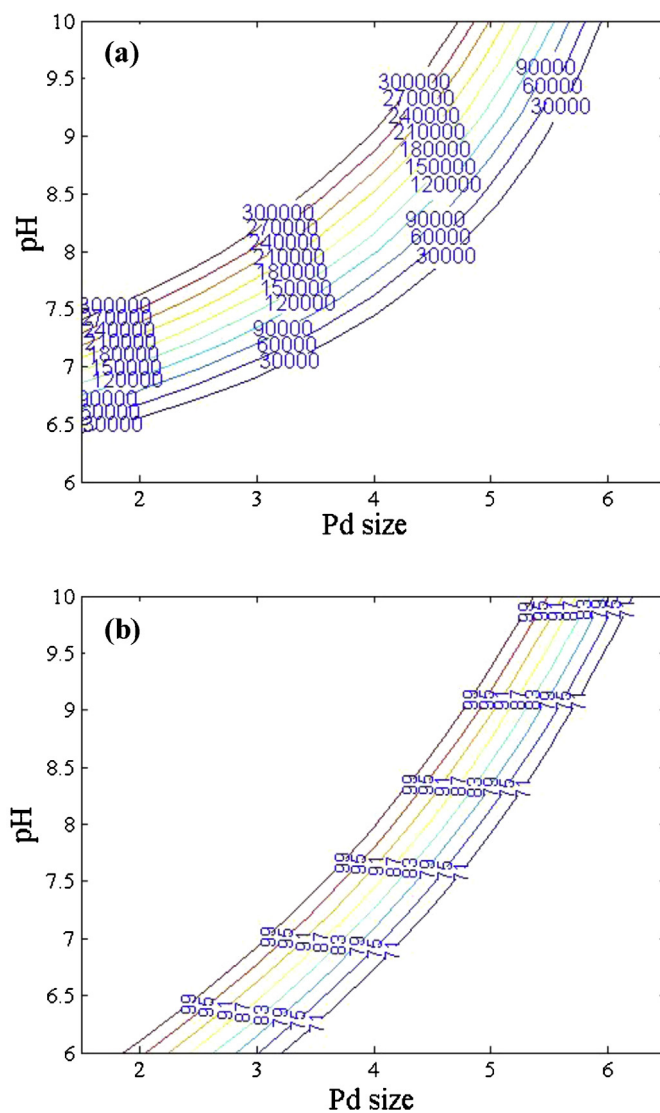

Fig. 14. Contour plots of (a) qTOF; (b) selectivity toward benzaldehyde with Pd size and pH as the variables.

Table 3
Effect of reaction condition s for 1Pd/2.4APS-CNT on benzyl alcohol oxidation.[a]

Entry	Temperature (°C)	O_2 flow rate (mL min^{-1})	Conversion (%)	Selectivity (%)		
				Benzaldehyde	Toluene	Benzoic acid
1	120	20	7.8	90.9	9.1	0
2	140	20	14.8	94.0	5.4	0.6
3	160	0	4.7	71.8	28.2	0
4	160	5	9.5	87.9	12.1	0
5	160	10	13.1	88.4	10.8	0.8
6	160	20	26.5	96.6	1.3	2.0
7	160	30	12.8	96.7	1.0	2.3

[a] Reaction conditions: benzyl alcohol/Pd = 1000 mol/g; reaction time = 1 h; stirring rate = 1200 rpm.
[b] TOF is defined following the equation in Section 2.3. Table 3 avoiding using qTOF since the qTOF might be negative when oxygen flow rate is zero.

investigated. The catalyst was recovered by washing with acetone and drying at 60 °C, and subsequently reused in the next run of reaction. Fig. 13 displays the recyclability of 1Pd/2.4APS-CNT for 5 consecutive reaction cycles. The loss of catalytic activity and selectivity is moderate for these five cycles, indicating that the loss of catalyst during recovery is insignificant. The Pd content after five consecutive cycles is almost the same as the as-produced catalyst with no leaching of Pd due to the strong metal–support interaction after modifying the CNT surfaces by APS. Therefore, APS-functionalized CNT supported Pd catalyst not merely improve the catalytic performance but also enhance the resistance against deactivation.

Upon hydrophilic amino-containing APS surface functionalization, palladium precursors are easily adsorbed, and Pd nanoparticles are uniformly immobilized on the surface-modified CNT support with a narrow size distribution and improved metal–support interaction along with the finely tuned basicity surrounding Pd nanoparticles. All these parameters are essential to account for the significantly improved catalytic performances, in which the surface basicity and Pd nanoparticle size are two crucial factors controlling the catalytic activity based on electro-active surface area (qTOF) and selectivity, The surface basicity also has impact on the Pd particle size and size distribution, leading to the complex and ambiguous explanation on the impact of individual factors and their interaction upon the catalytic behavior. To unravel the effects of each factor and their interaction with clarity, multivariate analysis modeling was applied to establish a second order polynomial regression with MATLAB to fit the two variables (x_1: Pd size, x_2: pH value) and two dependent variables (y_1: qTOF, y_2: selectivity toward benzaldehyde). The contour plots of qTOF and selectivity in Fig. 14 show a rational investigation of the effect of each experimental variable on the dependent variables. High qTOF can be obtained at small Pd size, along with mildly basic surfaces. Similarly, high selectivity can be achieved at small Pd size and mild basicity. Therefore, the controlling of Pd size and surface basicity influences the catalytic behavior.

4. Conclusions

Various organosilanes (APS, ATMS and HMDS) surface-functionalized CNT supported Pd catalysts were prepared following a post-synthesis grafting scheme along with a metal adsorption–reduction step. Catalytic performance of these as-synthesized catalysts has been examined in the solvent-free selective oxidation of benzyl alcohol with molecular oxygen. The results suggested that both the variety and amount of surface-functional groups on CNT support influenced the catalytic performance. An appropriate amount of APS surface-modified CNT supported Pd catalyst turned out to be the optimal catalyst as a result of the finely tuned surface basicity, small Pd particle size with narrow size distribution, high electron density and enhanced metal–support electronic

interaction. Among all these catalysts, 1Pd/2.4APS-CNT was explored with a remarkably high qTOF of 288,755 h^{-1} for benzyl alcohol oxidation.

References

[1] G.J. Hutchings, Chem. Commun. (2008) 1148–1164.
[2] K. Mori, T. Hara, T. Mizugaki, K. Ebitani, K. Kaneda, J. Am. Chem. Soc. 126 (2004) 10657–10666.
[3] F. Li, Q.H. Zhang, Y. Wang, Appl. Catal. A: Gen. 334 (2008) 217–226.
[4] Q. Zhang, W. Deng, Y. Wang, Chem. Commun. 47 (2011) 9275–9292.
[5] W. Fang, J. Chen, Q. Zhang, W. Deng, Y. Wang, Chem. Eur. J. 17 (2011) 1247–1256.
[6] N. Lopez, T.V.W. Janssens, B.S. Clausen, Y. Xu, M. Mavrikakis, T. Bligaard, J.K. Norskov, J. Catal. 223 (2004) 232–235.
[7] T.V.W. Janssens, B.S. Clausen, B. Hvolbaek, H. Falsig, C.H. Christensen, T. Bligaard, J.K. Norskov, Top. Catal. 44 (2007) 15–26.
[8] C.N.R. Rao, G.U. Kulkarni, P.J. Thomas, P.P. Edwards, Chem. Eur. J. 8 (2002) 29–35.
[9] E. Roduner, Chem. Soc. Rev. 35 (2006) 583–592.
[10] M. Haruta, Nature 437 (2005) 1098–1099.
[11] M. Haruta, T. Kobayashi, H. Sano, N. Yamada, Chem. Lett. (1987) 405–408.
[12] M. Haruta, Catal. Today 36 (1997) 153–166.
[13] M. Haruta, Cattech 6 (2002) 102–115.
[14] G.C. Bond, D.T. Thompson, Catal. Rev. – Sci. Eng. 41 (1999) 319–388.
[15] Y.T. Chen, Z. Guo, T. Chen, Y.H. Yang, J. Catal. 275 (2010) 11–24.
[16] A. Gervasini, A. Auroux, J. Catal. 131 (1991) 190–198.
[17] M. Ai, T. Ikawa, J. Catal. 40 (1975) 203–211.
[18] M. Ai, J. Catal. 40 (1975) 318–326.
[19] M. Ai, J. Catal. 40 (1975) 327–333.
[20] M. Ai, S. Suzuki, J. Catal. 30 (1973) 362–371.
[21] T. Mallat, A. Baiker, Chem. Rev. 104 (2004) 3037–3058.
[22] T. Matsumoto, M. Ueno, N. Wang, S. Kobayashi, Chem. Asian J. 3 (2008) 196–214.
[23] B. Wang, M. Lin, T.P. Ang, J. Chang, Y.H. Yang, A. Borgna, Catal. Commun. 25 (2012) 96–101.
[24] V. La Parola, M.L. Testa, A.M. Venezia, Appl. Catal. B – Environ. 119 (2012) 248–255.
[25] C. Bronnimann, T. Mallat, A. Baiker, J. Chem. Soc. – Chem. Commun. (1995) 1377–1378.
[26] C.Y. Du, T.S. Zhao, Z.X. Liang, J. Power Sources 176 (2008) 9–15.
[27] P. Serp, E. Castillejos, ChemCatChem 2 (2010) 41–47.
[28] C.M. Zhou, Y.T. Chen, Z. Guo, X. Wang, Y.H. Yang, Chem. Commun. 47 (2011) 7473–7475.
[29] H.T. Tan, Y.T. Chen, C.M. Zhou, X.L. Jia, J.X. Zhu, J. Chen, X.H. Rui, Q.Y. Yan, Y.H. Yang, Appl. Catal. B – Environ. 119 (2012) 166–174.
[30] V. Lordi, N. Yao, J. Wei, Chem. Mater. 13 (2001) 733–737.
[31] Y.-S. Chi, H.-P. Lin, C.-Y. Mou, Appl. Catal. A: Gen. 284 (2005) 199–206.
[32] S.L. Tian, H. Mo, R.F. Zhang, P. Ning, T.H. Zhou, Adsorpt. – J. Int. Adsorpt. Soc. 15 (2009) 477–488.
[33] H. Sun, Q.H. Tang, Y. Du, X.B. Liu, Y. Chen, Y.H. Yang, J. Colloid Interface Sci. 333 (2009) 317–323.
[34] S. Wu, Q. He, C. Zhou, X. Qi, X. Huang, Z. Yin, Y. Yang, H. Zhang, Nanoscale 4 (2012) 2478–2483.
[35] L. Xu, J.H. Fu, J.R. Schlup, J. Am. Chem. Soc. 116 (1994) 2821–2826.
[36] C.C. Perry, X.C. Li, J. Chem. Soc. – Faraday Trans. 87 (1991) 761–766.
[37] X.B. Liu, Z. Guo, S. Gunasekaran, C.B. Ching, Y. Chen, S.S.J. Leong, Y.H. Yang, Micropor. Mesopor. Mater. 122 (2009) 114–120.
[38] R. Jacquemin, S. Kazaoui, D. Yu, A. Hassanien, N. Minami, H. Kataura, Y. Achiba, Synth. Met. 115 (2000) 283–287.

[39] Z.G. Duan, W.H. Liao, G.H. Zhou, Adv. Condens. Matter Phys. 2010 (2010) 1–6, Article ID 258019.
[40] X.B. Wu, P. Chen, J. Lin, K.L. Tan, Int. J. Hydrogen Energy 25 (2000) 261–265.
[41] E.N. Konyushenko, J. Stejskal, M. Trchova, J. Hradil, J. Kovarova, J. Prokes, M. Cieslar, J.Y. Hwang, K.H. Chen, I. Sapurina, Polymer 47 (2006) 5715–5723.
[42] Y.K. Kim, H. Park, Energy Environ. Sci. 4 (2011) 685–694.
[43] H.G. Jiang, M. Ruhle, E.J. Lavernia, J. Mater. Res. 14 (1999) 549–559.
[44] A.L. Patterson, Phys. Rev. 56 (1939) 978–982.
[45] B. Lee, Z. Ma, Z.T. Zhang, C. Park, S. Dai, Micropor. Mesopor. Mater. 122 (2009) 160–167.
[46] A. Gniewek, A.M. Trzeciak, J.J. Ziółkowski, L. Kępiński, J. Wrzyszcz, W. Tylus, J. Catal. 229 (2005) 332–343.
[47] Z. Guo, Y.T. Chen, L.S. Li, X.M. Wang, G.L. Haller, Y.H. Yang, J. Catal. 276 (2010) 314–326.
[48] I.G. Casella, J. Electrochem. Soc. 155 (2008) D723–D729.
[49] C. Saravanan, N.M. Markovic, M. Head-Gordon, P.N. Ross, J. Chem. Phys. 114 (2001) 6404–6412.
[50] L.L. Fang, Q.A. Tao, M.F. Li, L.W. Liao, D. Chen, Y.X. Chen, Chin. J. Chem. Phys. 23 (2010) 543–548.
[51] S.X. Wu, Q.Y. He, C.M. Zhou, X.Y. Qi, X. Huang, Z.Y. Yin, Y.H. Yang, H. Zhang, Nanoscale 4 (2012) 2478–2483.
[52] C. Keresszegi, D. Ferri, T. Mallat, A. Baiker, J. Phys. Chem. B 109 (2005) 958–967.
[53] T. Mallat, A. Baiker, Catal. Today 19 (1994) 247–283.
[54] C.G. Swain, A.L. Powell, W.A. Sheppard, C.R. Morgan, J. Am. Chem. Soc. 101 (1979) 3576–3583.
[55] D.V. Leff, L. Brandt, J.R. Heath, Langmuir 12 (1996) 4723–4730.
[56] X. Feng, G.E. Fryxell, L.Q. Wang, A.Y. Kim, J. Liu, K.M. Kemner, Science 276 (1997) 923–926.
[57] D.P. Upare, S. Yoon, C.W. Lee, Korean J. Chem. Eng. 28 (2011) 731–743.
[58] D.I. Enache, J.K. Edwards, P. Landon, B. Solsona-Espriu, A.F. Carley, A.A. Herzing, M. Watanabe, C.J. Kiely, D.W. Knight, G.J. Hutchings, Science 311 (2006) 362–365.
[59] Y.T. Chen, H.M. Lim, Q.H. Tang, Y.T. Gao, T. Sun, Q.Y. Yan, Y.H. Yang, Appl. Catal. A: Gen. 380 (2010) 55–65.
[60] Q.H. Tang, Q.H. Zhang, H.L. Wu, Y. Wang, J. Catal. 230 (2005) 384–397.